Elucidating the Shape of Current Transients in Electrochemical Resistive-Pulse Sensing of Single Liposomes

Rujia Liu[†], Rui Jia[‡,§], Dengchao Wang*[,†], Michael V. Mirkin*[,‡,§]

[†]School of Chemical Sciences, University of Chinese Academy of Sciences, Beijing 100049, P. R. China

[‡]Department of Chemistry and Biochemistry, Queens College -CUNY, Flushing, New York 11367, United States

[§]The Graduate Center of City University of New York, New York, New York 10016, United States

ABSTRACT: Electrochemical resistive-pulse (ERP) sensing with conductive carbon nanopipettes (CNPs) has recently been developed and employed for detection of single liposomes, biological vesicles, and analysis of redox molecules contained in such vesicles. However, the origins of different shapes of current transients produced by translocation of single vesicles through the CNP remain poorly understood. Herein, we report extensive finite-element simulations of both portions of an ERP transient – the current blockage by a vesicle approaching and passing through the pipette orifice and the faradaic current spike due to oxidation/reduction of redox species released from a vesicle on the carbon surface – for different values of parameters defining the geometry and dynamics of the vesicle/CNP system. The effects of the pipette geometry, surface charge, transport, vesicle trajectory, and collision location on the shape of current transients are investigated. The possibility of quantitative analysis of experimental ERP transients produced by translocations of liposomes and extracellular vesicles by fitting them to simulated curves is demonstrated. The developed theory can enable more reliable interpretation of complicated ERP signals and characterization of the size and contents of single biological and artificial vesicles.

Many biologically important molecules are stored in and released from vesicles, such as synaptic vesicles[1, 2] and exosomes.[3] A typical example is oxidative stress components, *i.e.*, reactive oxygen and nitrogen species (ROS/RNS) produced in phagolysosomes of macrophage cells.[4] Revealing the physicochemical features of vesicles, including the size, surface charge, and the nature and concentration of encapsulated species, is essential for understanding and regulating cell functions and important physiological and pathological processes. Single vesicle analysis rather than bulk measurements is required to characterize the heterogeneity of vesicle population and assess the variability of their properties.[5, 6]

Along with the optical and microscopy techniques, various single entity methods, including resistive-pulse sensing,[7-9] collision techniques,[10-13] nanopipette-based electrochemical sensors,[14, 15] and their combinations[16, 17] have been used to detect and quantify single lipid vesicles either in solution or in living cells. The size and surface charge of a vesicle can be found from the resistive-pulse signal, while the amounts of encapsulated redox species can be evaluated from electrochemical collision current spike. We have recently introduced electrochemical resistive-pulse (ERP) sensing with conductive carbon nanopipettes (CNPs) for detection of a single vesicle and analysis of redox molecules contained in its cavity.[18] By using a CNP as a scanning electrochemical microscopy (SECM) tip[19][18][19], one can insert it inside a living cell to detect intracellular vesicles[20] or position near a cell surface to probe the extracellular vesicles[21] produced by a specific cell.

The hypothesized mechanism of the vesicle translocation though a CNP and collision with the carbon-coated inner pipette wall is shown in Scheme 1A. Once a CNP is put in the solution containing a redox mediator, the combination of its spherical diffusion to the pipette orifice with the fast thin-layer mass-transfer inside the pipette cavity results a steady-state faradaic current.[22, 23] Assuming a vesicle contains the reduced form of redox species (R), the current transient in this case is

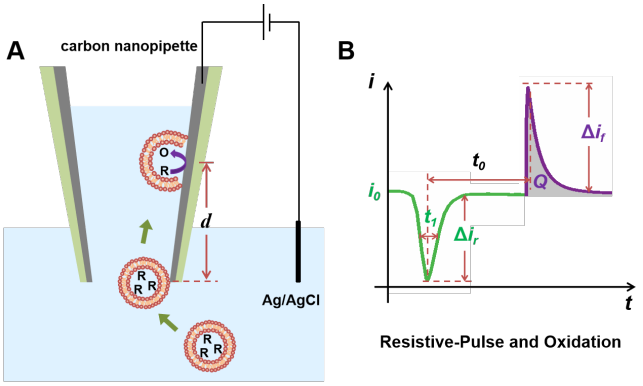

Scheme 1. Electrochemical resistive pulse sensing of single vesicles with a carbon nanopipette. (A) A vesicle containing redox species translocates through the CNP orifice and collides with its inner wall. (B) A transient decrease in the diffusion current (Δi_r) by the vesicle blocking of the CNP orifice and a faradaic current spike (Δi_f) produced by oxidation/reduction of the redox species released after its rupture. Not to scale.

expected to include a current blockage (green peak in Scheme 1B) and a faradaic current spike caused by oxidation of R released during the collision (purple peak).[19]

The amplitude of the ERP (Δi_r) and the faradaic charge(Q) can be correlated to the vesicle size and the amount of encapsulated redox species, respectively; while the concentration of vesicles in solution can be evaluated from the frequency of the current transients.[17, 24] The half-width of the ERP (t_1) is related to the translocation velocity,[25] and the amplitude of the faradaic spike (Δi_f) depends on dynamics of cargo release from the vesicle inside the CNP.[26, 27] Although the feasibility of ERP measurements of single vesicles has been demonstrated,[21, 28] no comprehensive theoretical description of current transients is currently available. In the simplified model (Scheme 1) used for experimental data analysis in earlier publications,[19-21] a vesicle enters the pipette in the center of its orifice, and its cargo is released through the complete and instantaneous membrane rupture. Other possible translocation/release scenarios result in a variety of shapes of current transients that remain poorly understood.

Here we use liposomes—spherical lipid bilayer structures with an inner cavity—as a model of biological vesicles to investigate various features of ERP transients and develop a more complete theory for this method. Liposomes are often employed as a model of biological vesicles because they can be precisely controlled, manipulated, and loaded with a wide range of cargo molecules.[29] They have also attracted a significant interest because of their applications to drug delivery.[30] We carried out finite-element simulations of ERPs and faradaic current spikes produced by single liposomes loaded with redox species and compared our computational results to experimental current transients to elucidate the effects of CNP size, half-cone angle, surface charge, transport direction, and liposome/CNP collision (*i.e.*, collision location and either complete rupture or partial opening of the vesicle).

Experimental Section

Chemicals and materials. Pegylated remote loadable liposomes were purchased from Avanti Polar Lipids and stored at -20 ℃. Aqueous solutions were prepared using deionized water from the Milli-Q Advantage A10 system (Millipore Corp.) equipped with Q-Gard T2 Pak, a Quantum TEX cartridge and a VOC Pak with total organic carbon (TOC) ≤ 1 ppb. Phosphate buffered saline tablet and potassium ferrocyanide ($K_4Fe(CN)_6$) were obtained from Sigma-Aldrich.

Fabrication of CNPs. CNPs were fabricated according to a previously reported protocol.[19,22] Briefly, a quartz capillary was pulled into two open nanopipettes using a laser pipet puller (P-2000, Sutter Instrument). The chemical vapor deposition was carried out to deposit a thin layer of carbon on the nanopipette inner wall in a mixed gas atmosphere of methane and nitrogen for 20 min at 950 ℃.

Preparation of liposomes containing redox molecules. Similar to the previously reported protocol,[19] 25 µL pegylated remote loadable liposomes (Avanti Polar Lipids) was mixed with 2.5 mL aqueous solution containing 100 mM $K_4Fe(CN)_6$ and 5 mM PBS in a glass vial. The mixture was then incubated at 55 ℃ for 4 hours. After cooling to room temperature, it was filtered through a PD-10 desalting column (Cytiva) using 10 mM PBS buffer to elute the $K_4Fe(CN)_6$ in the external solution.

Electrochemical resistive pulse sensing of liposomes. In ERP experiments, a small amount of solution was drawn into the CNP by capillary forces. A two-electrode setup included a CNP serving as the working electrode and an Ag/AgCl external reference electrode (Scheme 1). ERP experiments were carried out with a patch clamp amplifier (Multiclamp 700B, Molecular Devices Corporation) in the voltage-clamp mode. A Digidata 1550A analog-to-digital converter (Molecular Devices) was used to digitize the signal at a sampling frequency of 100 kHz and a 2 kHz low pass filter. The data was analyzed by pClamp 10 software (Molecular Devices).

After ERP experiments, the size and geometry of CNPs were characterized by TEM (JEOL TEM-2100 Instrument) with a relatively low-energy electron beam (80 kV voltage). A nanopipette was attached to the TEM grid (PELCO SynapTek™ DOT Grids, 1 x 2 mm slot, Beryllium-Copper). The tip of the pipette was positioned to be visible within the central hole of the grid, and the remaining portion of the pipette was subsequently cut off.

Simulation methods. Finite-element simulations of ion transport processes in electrochemical and resistive pulse sensing experiments were performed using a commercial software package COMSOL Multiphysics 5.4 with a 3D-model. The mass transport processes in solution were described by the Nernst-Planck equation:

$$J_i = -D_i \nabla c_i - \frac{z_i F}{RT} D_i \nabla c_i \nabla \phi \qquad (1)$$

where J_i is the total flux, D_i, c_i, and z_i is the diffusion coefficient, concentration, and valence of ionic species i, respectively. F is the Faraday constant, R is the gas constant, T is the temperature, and ϕ is the solution potential. The potential distribution in solution is calculated busing the Poisson equation:

$$\nabla^2(\varepsilon_0 \varepsilon_r \phi) = -\mathrm{F} \sum z_i c_i \qquad (2)$$

where ε_0, ε_r are the relative permittivity of the vacuum and medium respectively. Initially, the concentration of the electroactive species (c_R) inside the liposome is set as 500 mM, while that outside the liposome was 10 mM.

At the electrode/solution interface, the flux of the redox molecules follows the Butler-Volmer equation with Frumkin correction[31]:

$$J_R = k^0 c_O e^{-\alpha f(E-\phi-E^{0'})} - k^0 c_R e^{(1-\alpha) f(E-\phi-E^{0'})} \qquad (3)$$

$$J_O = -k^0 c_O e^{-\alpha f\left(E-\phi-E^{0'}\right)} + k^0 c_R e^{(1-\alpha) f(E-\phi-E^{0'})} \qquad (4)$$

where k^0 = 10 cm/s is the standard rate constant and $E^{0'}$ = 0.1V is formal potential for the ET process. $f = zF/RT$, and α is the transfer coefficient. E = 0.5 V is the applied potential here.

The resulting current is obtained by integrating the flux of the redox molecules at the carbon electrode surface:

$$i = \int F J_R \mathrm{d}S \qquad (5)$$

where F is the Faraday constant, S is the electrode surface.

Additional simulation details can be found in the COMSOL simulation report (Supporting Information).

Results and Discussion

Simulated dimensionless current *vs.* displacement curves (Figure 1A) for a liposome with the radius r_l approaching and entering a carbon nanopipette along its axis (vesicle 1 in Figure 1C) in solution containing the reduced form of redox species show that the steady-state oxidation current begins to decrease at the separation distance, $z \approx 3a$ (a is the CNP orifice radius) and returns to the original value at $z \approx -1a$, with a vesicle inside the pipette. The translocation produces an ERP with the minimum current value occurring when the vesicle center is close to the pipette orifice ($z \approx 0$). The current decrease results from the blockage of the diffusional flux of redox mediator toward the carbon surface (Figure 1C). One should notice the increased flux at the edges of the nanopipette, as the flux at the carbon ring is the main source of the steady-state current at the CNPs.[23] As expected, the larger the r_l, the larger the corresponding Δi_r value: e.g., a 0.6% decrease ($\Delta i_r/i_0$) corresponds to $r_l = 1/4a$, while a 56% decrease is obtained when $r_l = a$. (No liposome with $r_l > a$ can translocate through the CNP orifice).

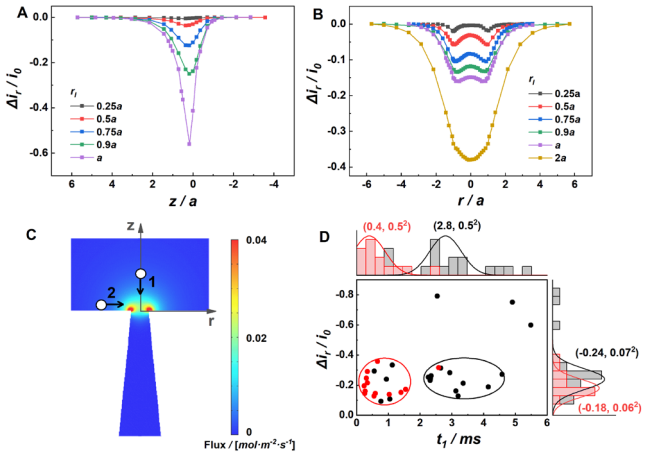

Figure 1. Simulated current transients for ERP sensing of single liposomes. (A, B) Dependence of the ERP shape on r_l for (A) translocating vesicles and (B) vesicles traveling in the plane parallel to the CNP orifice ($z = r_l$). The coordinates of the center of the orifice are r = 0, z = 0. (C) Simulated flux distribution for a diffusion-limited oxidation of reduced redox species at the CNP surface. The trajectories of liposomes translocating through the CNP (1) and traveling laterally (2) are indicated by arrows. a = 140 nm, tanθ = 0.1, c_R = 10 mM, D = 7.6 x 10^{-6} cm^2/s; the carbon film thickness is 5 nm. (D) Histograms of ERP amplitude and half-width time obtained from experimental type 1 (black points) and type 2 (red points) transients in the current recording shown in Figure S1 (the experimental data is from ref. 21). Solution contained 10 mM $K_4Fe(CN)_6$ and 10 mM PBS. a = 207 nm.

The diffusion current blockage can also occur when a vesicle passes laterally near the CNP orifice without entering the pipette (vesicle 2 in Figure 1C). Larger vesicles are expected to cause larger current drop ($\Delta i_r/i_0$; Figure 1B), and the vesicles with $r_l > a$, can produce significant ERP signal, contrary to the earlier assumption.[19]

Experimental ERP current-time recordings obtained with extracellular vesicles[21] comprised two types of current transients: (1) a resistive pulse followed by a faradaic current spike and (2) a resistive pulse only. The simulation results in Figure 1 suggest that the type 1 transients were produced by vesicles translocating through the CNP orifice, while type 2 transients represent vesicles that approached the CNP orifice laterally and did not translocate. To check this hypothesis, we analyzed the current-time recordings obtained with a platinized CNP positioned near the breast cell surface to detect the released extracellular vesicles[21] (Figure S1; Supporting Information). The histograms obtained from such recordings (Figure 1D) show the distributions of the ERP half-width (t_1) and the extent of current blockage for type 1 (black dots) and type 2 (red dots) transients. As expected from simulations, type 2 transients display smaller current blockages (-0.18 ± 0.06) and shorter t_1 (0.4 ± 0.5 ms) than those obtained from type 1 transients (i.e., -0.24 ± 0.07 and 2.8 ± 0.5 ms, respectively).

We used the experimental ERP data obtained with model liposomes to show he possibility of evaluating the size of the vesicles from the ERP amplitude ($\Delta i_r/i_0$). In Figure 2, three experimental ERP transients (black curves) were fitted to simulated curves (red dots) by using the liposome radius (r_l) as the fitting parameter. With the CNP radius, a = 50 nm, the r_l values found from the fit are within the range 37.5 nm to 50 nm, which brackets the nominal liposome radius (45 nm) reported by the manufacturer. It is worth pointing out the COMSOL simulations yield ERP current as a function of liposome coordinate.

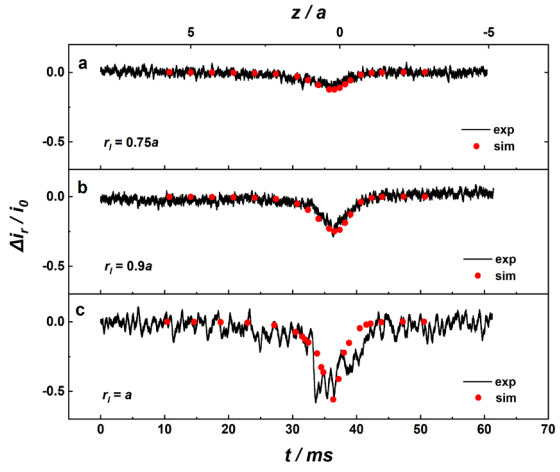

Figure 2. Fitting experimental ERPs produced by single liposomes to the theory. Experimental and simulation parameters: a = 50 nm, tanθ = 0.1, carbon film thickness = 5 nm, c_R = 10 mM, D = 7.6 x 10^{-6} cm^2/s; solution contained 10 mM $K_4Fe(CN)_6$ and 10 mM PBS.

To fit the experimental ERPs to these curves, the simulated position values were converted to the time scale using an estimate for the liposome velocity, 148 μm/s, which is comparable to the previously reported values.[32, 33] Then, the simulated steady-state current responses at a given vesicle coordinate can be used to approximately fit the overall shape of the experimental current transients. We also used this approach to evaluate the size of the vesicles released from breast cells (Figures S1 and 1D). From the average $\Delta i_r/i_0$ = -0.24, $r_l \approx 0.9a$ (where a = 207 nm), *i.e.*, 186 nm.

Other factors, such as the radial coordinate of the liposome center during its translocation, the pipette inside geometry, and charge density on carbon surface, may affect the shape of ERP current transients. The blockage effect of a liposome as a function of its r coordinate is shown in Figure S3. Qualitatively, the liposome translocation along the carbon surface should result in a larger current drop than that along the CNP axis. However, this effect is relatively small (much smaller than the effect of the r_l value; cf. Figure 1A) and should only slightly increase the variability of ERP transients. The effects of the half-cone angle (θ; Figure S4) and surface charge density of the inner carbon layer (Figure S5) on the extent of the current blockage, are essentially negligible.

Unlike conventional asymmetrical resistive pulses with the sharp initial decrease in current followed by a slow relaxation "tail"[25, 34, 35] (see also Figure S6), simulated ERPs are essentially symmetrical. This difference reflects different origins of conventional and electrochemical resistive pulses: the former are caused by the increased resistance of the pipette during the particle translocation, while the latter are due to hindered diffusion of redox species to the CNP orifice. The conical pipette resistance is largely determined by the inner region adjacent to its orifice (-0.15a < z < 0); therefore, the half-cone angle, surface charge density, and solution ionic strength greatly influence the shape of conventional resistive pulses.[25, 33-37] By contrast, the ERP signals shown here are mainly determined by a and r_l, and the effects of the pipette inside geometry and surface charge density are small, allowing for simpler and more reliable analysis of the experimental curves.

It was assumed previously[19-21] that after translocating across the CNP orifice, a vesicle quickly collides with its inner wall, bursts, and releases all its cargo (*e.g.,* ROS/RNS), which reacts at the carbon surface, producing a faradaic current spike. However, TEM images of CNPs after resistive-pulse experiments with liposomes (Figure 3A) showed that a vesicle may remain intact inside the pipette and in contact with the carbon surface. (Long ERP transients with the current dropping to near-zero due to the complete CNP blockage by a large liposome have been reported previously[19]). Thus, a vesicle can travel a significant distance inside the pipette before opening and releasing its contents, and the shape of the resulting faradaic spike may depend on the collision location relative to the pipette orifice.

Figure 3B shows faradaic current spikes simulated for different d values (d is the z-coordinate of the vesicle center at the

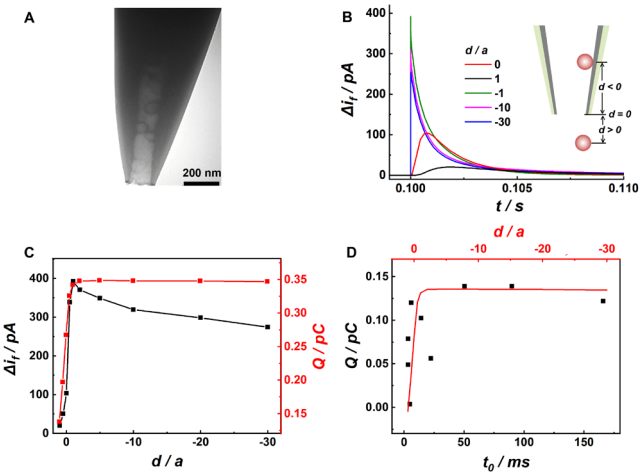

Figure 3. (A) TEM image of liposomes inside a carbon nanopipette. (B) Simulated i-t responses for liposome cargo release near the inner CNP wall at different distances from the pipette orifice. (C) Simulated dependences of the peak current and transferred charge on the penetration depth at the moment of the vesicle rupture. (D) Experimental dependence of the transferred charge vs. delay time (black points) obtained from single vesicle transients (Figure S1) fitted to the simulated data (red line). Simulation parameters: a = 240 nm, r_l = 120 nm, tanθ = 0.1, carbon thickness = 5 nm, c_R = 0.5 M, $D = 7.6 \times 10^{-8}$ cm^2/s.

moment of its rupture; Scheme 1A). The peak current (Δi_f) is significantly lower, and the spike duration is longer if $d \geq 0$, *i.e.*, the vesicle is not entirely inside the CNP when its cargo is released, because the redox species have to diffuse to the carbon surface from the outer solution. The spike is much higher and narrower at d = -a, and its height somewhat decreases with increasing collision depth because the inner CNP radius increases with increasing distance from the orifice (black curve in Figure 3C). To simulate these transients, we assumed that the diffusion coefficient of redox species inside the vesicle is two orders of magnitude lower than in the buffer solution.[38, 39] Although the shape and duration of simulated spikes are consistent with those observed experimentally,[19-21] the assumed diffusion coefficient value is hard to validate because after the liposome opening its contents mix with the external buffer solution. The simulated Δi_f vs d dependence is only semi-quantitative.

The total amount of redox species released from a liposome can be evaluated from the charge value (Q; Scheme 1B) obtained by integrating the current for the corresponding spike. If $d \geq 0$, a fraction of the released redox species diffuse away from the CNP, whereas if a liposome bursts inside the pipette, all redox molecules reach the carbon wall. Thus Q increases with penetration depth and then levels off at the value corresponding to the total amount of encapsulated electroactive molecules (red curve in Figure 3C). As the threshold Q value represents the total amount of encapsulated electroactive molecules, it is independent of the pipette size, as confirmed by the overlapping faradic spikes simulated for different CNP radii (Figure S7).

Because the *d* values for experimental current spikes are not directly accessible, we used the delay time between the blockage and the current maximum (t_0 in Scheme 1B, Figure S8 shows the histogram of t_0 values) as a measure of the collision depth inside a CNP. Here, only these events with well separated negative and positive peaks ($t_0 > 2$ ms) are used to calculate Q, as the overlap between ERP and oxidation peaks could alter the Q values. The estimated liposome velocity from Figure 2 (148 µm/s) was used to convert simulated Q vs. *d* curves to the time scale (solid curve in Figure 3D). This curve is in good agreement with experimental data points (symbols in Figure 3D) obtained for vesicles released from a breast cell,[21] suggesting that the charge values measured at longer t_0 can be used to quantify the redox species contained in individual vesicles.

The possibility of slow or partial release of the cargo from liposomes and biological vesicles (as opposed to the instantaneous full rupture) has been discussed in several publications.[19, 26, 27, 38-40] Lower amplitude spikes with a longer duration in ERP recordings[21] may represent partial release of vesicle contents via slow diffusion through a nanopore.[40] The current−time responses were simulated for a range of pore radii and locations on the liposome surface relative to the CNP's inner wall (Figure 4). The angle α defining the pore location (Figure 4A) varies from 0° (the pore in the liposome faces the carbon surface) to 180° (the pore center is at the opposite end of the liposome diameter perpendicular to the inner wall). As expected, for a fixed pore radius (e.g., 40 nm in Figure 4A), the highest and sharpest current spike occurs at α = 0°, and the

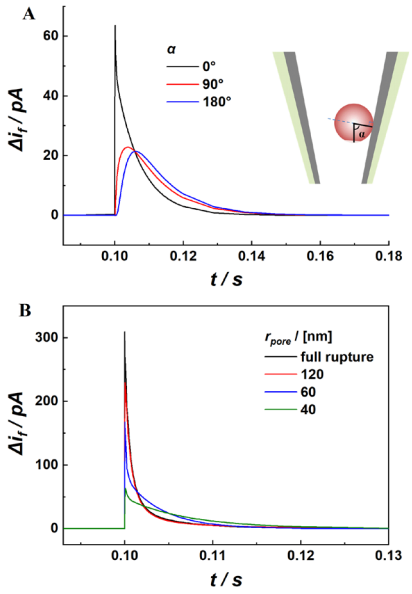

Figure 4. *i-t* responses simulated for the release of redox species through the nanopore formed in a liposome touching the inner CNP wall for (A) the different pore positions and constant radius of 40 nm, and (B) different pore radii at α = 0°. The α value defines the position of the pore center relative to the inner wall. a = 240 nm, r_l = 120 nm, d = -10a, tanθ = 0.1, D = 7.6 × 10^{-8} cm^2/s, c_R = 0.5 M.

current peak becomes lower and broader with increasing α, as the redox species need more time to arrive to the electrode surface and get oxidized.

The effect of the pore radius on faradaic current spikes is shown in Figure 4B. The peak becomes narrower, and its amplitude increases as the pore radius increases from 40 nm to 120 nm. Overall, a broader oxidation peak is expected for a smaller pore in the liposome located further from the carbon surface. The distribution of oxidation peak half-widths obtained from an experimental ERP current recording (Figure S9) shows these effects. While the analysis of the experimental faradaic current spikes is challenging because of the large number of factors affecting their shape, the total charge obtained by current integration is independent of pore radius, angle α, and the collision depth inside a CNP, which enables the quantitative analysis of redox species encapsulated in single vesicles.

Conclusions

In conclusion, we used numerical simulations to elucidate the features of current transients produced by translocations of single liposomes through CNPs in electrochemical resistive-pulse experiments. Unlike conventional resistive-pulse sensing, the current blockages in ERP recordings are essentially symmetrical and almost independent of the pipette inside geometry, surface charge density, and trajectory of a translocating vesicle. The extent of current blockage is mainly determined by the liposome and CNP radii and can be used to evaluate the vesicle size. By contrast, the complicated shape of spikes produced by the electrolysis of redox species released from a single vesicle is influenced by several factors, including the depth of collision position, the mechanism of cargo release from the vesicle (i.e., full rupture vs. nanopore formation), and mass-transfer rate, which hinder quantitative analysis of current transients. The total charge transferred during the electrolysis of released redox species is largely independent of those factors and suitable for quantifying the contents of single liposomes and biological vesicles.

ASSOCIATED CONTENT

Supporting Information

Additional simulated current transients and histograms for experimental faradaic current spikes, including simulation details, Figures S1−S9, Tables 1 and 2, and COMSOL simulation report (PDF). This material is available free of charge via the Internet at http://pubs.acs.org.

AUTHOR INFORMATION

Corresponding Authors

Dengchao Wang - *School of Chemical Sciences, University of Chinese Academy of Sciences, Beijing 100049, P. R. China; orcid.org/0000-0002-4909-7830;*

Email: wangdengchao@ucas.ac.cn

Michael V. Mirkin - *Department of Chemistry and Biochemistry, Queens College, Flushing, New York 11367, United States; Advanced Science Research Center at The Graduate Center, CUNY, New York, New York 10031, United States; orcid.org/0000-0002-3424-5810;*
Email: mmirkin@qc.cuny.edu

Authors

Rujia Liu - *School of Chemical Sciences, University of Chinese Academy of Sciences, Beijing 100049, P. R. China;*

Rui Jia - *Department of Chemistry and Biochemistry, Queens College, Flushing, New York 11367, United States; Advanced Science Research Center at The Graduate Center, CUNY, New York, New York 10031, United States; orcid.org/0000-0002-6094-982X;*

Author Contributions

All authors have given approval to the final version of the manuscript.

Notes

The authors declare no competing financial interest.

ACKNOWLEDGMENTS

The support of this work National Natural Science Foundation of China (21904126) and Fundamental Research Funds for the Central Universities (D.W.)., and the National Science Foundation grant CHE-2102298 (M.V.M.) is gratefully acknowledged.

REFERENCES

(1) Phan, N. T. N.; Li, X.; Ewing, A. G., Measuring Synaptic Vesicles Using Cellular Electrochemistry and Nanoscale Molecular Imaging. *Nat. Rev. Chem.* **2017,** *1,*1-18.
(2) Stevens, C. F. Neurotransmitter Release at Central Synapses. *Neuron* **2003**, *40*, 381-388.
(3) Kalluri, R.; LeBleu, V. S., The Biology, Function, and Biomedical Applications of Exosomes. *Science* **2020,** *367,* 6478.
(4) Gordon, S., Phagocytosis: An Immunobiologic Process. *Immunity* **2016,** *44*, 463-475.
(5) Pick, H.; Alves, A. C.; Vogel, H., Single-Vesicle Assays Using Liposomes and Cell-Derived Vesicles: From Modeling Complex Membrane Processes to Synthetic Biology and Biomedical Applications. *Chem. Rev.* **2018,** *118*, 8598-8654.
(6) Bordanaba-Florit, G.; Royo, F.; Kruglik, S. G.; Falcón-Pérez, J. M., Using Single-Vesicle Technologies to Unravel the Heterogeneity of Extracellular Vesicles. *Nat. Protoc.* **2021,** *16*, 3163-3185.
(7) Darvish, A.; Goyal, G.; Aneja, R.; Sundaram, R. V.; Lee, K.; Ahn, C. W.; Kim, K. B.; Vlahovska, P. M.; Kim, M. J., Nanoparticle Mechanics: Deformation Detection Via Nanopore Resistive Pulse Sensing. *Nanoscale* **2016,** *8*, 14420-14431.
(8) Vogel, R.; Coumans, F. A.; Maltesen, R. G.; Boing, A. N.; Bonnington, K. E.; Broekman, M. L.; Broom, M. F.; Buzas, E. I.; Christiansen, G.; Hajji, N.; Kristensen, S. R.; Kuehn, M. J.; Lund, S. M.; Maas, S. L.; Nieuwland, R.; Osteikoetxea, X.; Schnoor, R.; Scicluna, B. J.; Shambrook, M.; de Vrij, J.; Mann, S. I.; Hill, A. F.; Pedersen, S., A Standardized Method to Determine the Concentration of Extracellular Vesicles Using Tunable Resistive Pulse Sensing. *J Extracell Vesicles* **2016,** *5*, 31242.
(9) Lane, R. E.; Korbie, D.; Anderson, W.; Vaidyanathan, R.; Trau, M., Analysis of Exosome Purification Methods Using a Model Liposome System and Tunable-Resistive Pulse Sensing. *Sci. Rep.* **2015,** *5*, 7639.
(10) Luy, J.; Ameline, D.; Thobie-Gautier, C.; Boujtita, M.; Lebegue, E., Detection of Bacterial Rhamnolipid Toxin by Redox Liposome Single Impact Electrochemistry. *Angew. Chem. Int. Ed.* **2022,** *61*, e202111416.
(11) Lebegue, E.; Barriere, F.; Bard, A. J., Lipid Membrane Permeability of Synthetic Redox Dmpc Liposomes Investigated by Single Electrochemical Collisions. *Anal. Chem.* **2020,** *92*, 2401-2408.
(12) Cheng, W.; Compton, R. G., Investigation of Single-Drug-Encapsulating Liposomes Using the Nano-Impact Method. *Angew. Chem. Int. Ed.* **2014,** *53*, 13928-13930.
(13) Hu, K.; Le Vo, K. L.; Wang, F.; Zhang, X.; Gu, C.; Fang, N.; Phan, N. T. N.; Ewing, A. G., Single Exosome Amperometric Measurements Reveal Encapsulation of Chemical Messengers for Intercellular Communication. *J. Am. Chem. Soc.* **2023,** *145*, 11499-11503.
(14) Huang, L.; Zhang, J.; Xiang, Z.; Wu, D.; Huang, X.; Huang, X.; Liang, Z.; Tang, Z. Y.; Deng, H., Faradaic Counter for Liposomes Loaded with Potassium, Sodium Ions, or Protonated Dopamine. *Anal. Chem.* **2021,** *93*, 9495-9504.
(15) Lu, S. M.; Peng, Y. Y.; Ying, Y. L.; Long, Y. T., Electrochemical Sensing at a Confined Space. *Anal. Chem.* **2020,** *92*, 5621-5644.
(16) Pan, R.; Xu, M.; Burgess, J. D.; Jiang, D.; Chen, H. Y., Direct Electrochemical Observation of Glucosidase Activity in Isolated Single Lysosomes from a Living Cell. *Proc. Natl. Acad. Sci. U. S. A.* **2018,** *115*, 4087-4092.
(17) Zhang, X. W.; Hatamie, A.; Ewing, A. G., Simultaneous Quantification of Vesicle Size and Catecholamine Content by Resistive Pulses in Nanopores and Vesicle Impact Electrochemical Cytometry. *J. Am. Chem. Soc.* **2020,** *142*, 4093-4097.
(18) Xu, X.; Valavanis, D.; Ciocci, P.; Confederat, S.; Marcuccio, F.; Lemineur, J. F.; Actis, P.; Kanoufi, F.; Unwin, P. R., The New Era of High-Throughput Nanoelectrochemistry. *Anal. Chem.* **2023,** *95*, 319-356.
(19) Pan, R.; Hu, K.; Jiang, D.; Samuni, U.; Mirkin, M. V., Electrochemical Resistive-Pulse Sensing. *J. Am. Chem. Soc.* **2019,** *141*, 19555-19559.
(20) Pan, R.; Hu, K.; Jia, R.; Rotenberg, S. A.; Jiang, D.; Mirkin, M. V., Resistive-Pulse Sensing inside Single Living Cells. *J. Am. Chem. Soc.* **2020,** *142*, 5778-5784.
(21) Jia, R.; Rotenberg, S. A.; Mirkin, M. V., Electrochemical Resistive-Pulse Sensing of Extracellular Vesicles. *Anal. Chem.* **2022,** *94*, 12614-12620.
(22) Yu, Y.; Noel, J. M.; Mirkin, M. V.; Gao, Y.; Mashtalir, O.; Friedman, G.; Gogotsi, Y., Carbon Pipette-Based Electrochemical Nanosampler. *Anal. Chem.* **2014,** *86*, 3365-3372.
(23) Liu, R.; Ma, Y.; Shen, X.; Wang, D., Quantification of the Charge Transport Processes inside Carbon Nanopipettes. *Chem. Sci.* **2021,** *12*, 14752-14757.
(24) Liu, Y.; Xu, C.; Yu, P.; Chen, X.; Wang, J.; Mao, L., Counting and Sizing of Single Vesicles/Liposomes by Electrochemical Events. *ChemElectroChem* **2018,** *5*, 2954-2962.
(25) Luo, L.; German, S. R.; Lan, W. J.; Holden, D. A.; Mega, T. L.; White, H. S., Resistive-Pulse Analysis of Nanoparticles. *Annu. Rev. Anal. Chem.* **2014,** *7*, 513-535.
(26) Li, X.; Ren, L.; Dunevall, J.; Ye, D.; White, H. S.; Edwards, M. A.; Ewing, A. G., Nanopore Opening at Flat and Nanotip Conical Electrodes During Vesicle Impact Electrochemical Cytometry. *ACS Nano* **2018,** *12*, 3010-3019.
(27) Zhang, X. W.; Oleinick, A.; Jiang, H.; Liao, Q. L.; Qiu, Q. F.; Svir, I.; Liu, Y. L.; Amatore, C.; Huang, W. H., Electrochemical Monitoring of Ros/Rns Homeostasis within Individual

Phagolysosomes inside Single Macrophages. *Angew. Chem. Int. Ed.* **2019,** *58*, 7753-7756.

(28) Hu, K.; Jia, R.; Hatamie, A.; Le Vo, K. L.; Mirkin, M. V.; Ewing, A. G., Correlating Molecule Count and Release Kinetics with Vesicular Size Using Open Carbon Nanopipettes. *J. Am. Chem. Soc.* **2020,** *142*, 16910-16914.

(29) Parchekani, J.; Allahverdi, A.; Taghdir, M.; Naderi-Manesh, H., Design and Simulation of the Liposomal Model by Using a Coarse-Grained Molecular Dynamics Approach Towards Drug Delivery Goals. *Sci. Rep.* **2022,** *12*, 2371.

(30) Pattni, B. S.; Chupin, V. V.; Torchilin, V. P., New Developments in Liposomal Drug Delivery. *Chem. Rev.* **2015,** *115*, 10938-10966.

(31) Bard, A. J.; Faulkner, L. R. Double-Layer Effects on Electrode Reaction Rates. *Electrochemical Methods: Fundamentals and Applications*, 2nd ed.; John Wiley & Sons: **2001**, pp 571-572.

(32) Liu, Y.; Xu, C.; Chen, X.; Wang, J.; Yu, P.; Mao, L., Voltage-Driven Counting of Phospholipid Vesicles with Nanopipettes by Resistive-Pulse Principle. *Electrochem. Com.* **2018,** *89*, 38-42.

(33) Holden, D. A.; Watkins, J. J.; White, H. S., Resistive-Pulse Detection of Multilamellar Liposomes. *Langmuir* **2012,** *28*, 7572-7577.

(34) Wang, Y.; Kececi, K.; Mirkin, M. V.; Mani, V.; Sardesai, N.; Rusling, J. F., Resistive-Pulse Measurements with Nanopipettes: Detection of Au Nanoparticles and Nanoparticle-Bound Anti-Peanut Igy. *Chem. Sci.* **2013,** *4*, 655-663.

(35) Heins, E. A.; Siwy, Z. S.; Baker, L. A.; Martin, C. R., Detecting Single Porphyrin Molecules in a Conically Shaped Synthetic Nanopore. *Nano. Lett.* **2005,** *5*, 1824-1829.

(36) Lan, W.-J.; Kubeil, C.; Xiong, J.-W.; Bund, A.; White, H. S., Effect of Surface Charge on the Resistive Pulse Waveshape During Particle Translocation through Glass Nanopores. *J. Phys. Chem. C* **2014,** *118*, 2726-2734.

(37) Qiu, Y.; Lin, C. Y.; Hinkle, P.; Plett, T. S.; Yang, C.; Chacko, J. V.; Digman, M. A.; Yeh, L. H.; Hsu, J. P.; Siwy, Z. S., Highly Charged Particles Cause a Larger Current Blockage in Micropores Compared to Neutral Particles. *ACS Nano* **2016,** *10*, 8413-8422.

(38) Li, X.; Majdi, S.; Dunevall, J.; Fathali, H.; Ewing, A. G., Quantitative Measurement of Transmitters in Individual Vesicles in the Cytoplasm of Single Cells with Nanotip Electrodes. *Angew. Chem. Int. Ed.* **2015,** *54*, 11978-11982.

(39) Amatore, C.; Bouret, Y.; Midrier, L. Time-Resolved Dynamics of the Vesicle Membrane During Individual Exocytotic Secretion Events, as Extracted from Amperometric Monitoring of Adrenaline Exocytosis from Chromaffin Cells. *Chem. Eur. J.* **1999**, *5*, 2151-2162.

(40) Lovric, J.; Najafinobar, N.; Dunevall, J.; Majdi, S.; Svir, I.; Oleinick, A.; Amatore, C.; Ewing, A. G., On the Mechanism of Electrochemical Vesicle Cytometry: Chromaffin Cell Vesicles and Liposomes. *Faraday Discuss* **2016,** *193*, 65-79.

Only for the Table of Contents